Table 2. Surgical History of Each Patient

Group	Patients	Indication of First Operation	Maximum Diameter of Aorta (mm)	First Operation	Second Operation		Third Operation		Fourth Operation		Fifth Operation		Total Aortic Replacement
D	1	Chronic AD (B)	60	DTAA repair	VSRR (remodeling) + TAR	(49)	TAAA repair	(53)	Bentall	(159)	...		Yes
	2	Chronic AD (B)	60	AAA repair	HAR	(5)	DTAA repair	(46)	TAAA repair	(85)	Bentall + TAR	(154)	Yes
	3	Chronic AD (B)	N/A	DTAA repair	TAR	(41)	TAAA repair	(62)	Bentall + MVR	(104)	...		Yes
	4	Chronic AD (B)	45	AAA repair	...		...		...		...		No
	5	Chronic AD (B)	60	TAR	AAA repair	(110)	TAAA repair	(116)	...		...		No
	6	Chronic AD (B)	59	DTAA repair	Bentall + TAR	(13)	TAAA repair	(26)	...		...		Yes
	7	Acute AD (A)	N/A	Bentall	TAR	(132)	RedoBentall	(195)	Redo Bentall	(196)	...		No
	8	Acute AD (A)	78	HAR	VSRR	(51)	...		...		...		No
	9	Acute AD (A)	N/A	HAR	VSRR + TAR	(67)	...		...		...		No
	10	Acute AD (A)	...	TAR	DTAA repair	(1)	...		...		...		No
N	11	AAE	57	VSRR	TAR	(79)	DTAA repair		AAA repair		TAAA repair		Yes
	12	AAE	50	VSRR	...		...		...		...		No
	13	AAE	45	VSRR	...		...		...		...		No
	14	AAE	48	VSRR	...		...		...		...		No
	15	AAE	58	VSRR	...		...		...		...		No
	16	AAE	60	VSRR	AAA repair	(3)	...		...		...		No

Numbers in parentheses indicate months from first operation.

AAA = abdominal aortic aneurysm; AAE = annuloaortic ectasia; AD (A) = aortic dissection, type A; AD (B) = aortic dissection, type B; DTAA = descending thoracic aortic aneurysm; HAR = hemiarch replacement; MVR = mitral valve replacement; N/A = not available; TAAA = thoracoabdominal aortic aneurysm; TAR = total arch replacement; VSRR = valve-sparing root replacement.

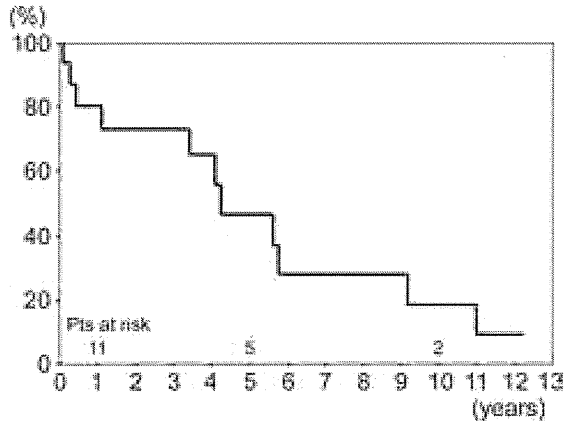

Fig 1. Freedom from aortic reintervention for all patients (Pts) after first aortic operation.

TGFBR molecules are associated with cardiovascular development and function: *TGFBR1* or *TGFBR2* mutations influence collagen deposition and elastin organization in the extracellular matrix. With respect to the histopathologic features of aortic specimens, fragmentation of elastic fibers is frequently seen in patients with both LDS and MFS. Maleszewski and colleagues [5], who examined aortic specimens of patients with both LDS and MFS in detail, showed that high collagen deposition and medial degeneration of the diffuse type with relatively little medial degeneration of the cystic type helps differentiate LDS from MFS. Indeed, in most of our patients, the pathologic findings showed diffuse medial degeneration in addition to fragmentation of elastic fibers. These changes in the media make the aortic wall fragile and lead to arterial tortuosity with aortic aneurysms and dissections.

In patients with LDS, management of aortic lesions is vital for prognosis, as it is in other CTDs. Most patients in group D, who underwent initial aortic repair after aortic dissection, needed further aortic operations because the dissected aorta of patients with LDS dilates easily. As a result, 40% of patients had their aortas replaced entirely in several rounds of aortic repair. Conversely, all patients in group N, in whom aortic lesions were detected before aortic events occurred, underwent aortic operations for AAE. For all patients in group N, VSRR with a reimplantation technique using a polyester tube graft with prefashioned pseudosinuses (Gelweave Valsalva graft; Vascutek, Renfrewshire, Scotland, UK) could be carried out successfully, and postoperative echocardiography revealed less than trivial aortic regurgitation. Patel and colleagues [6] demonstrated that midterm results of VSRR for patients with LDS are encouraging, and we also believe that it is an effective surgical option, especially for young patients.

In our series, there were 2 cases of subdural hematoma postoperatively. One occurred after descending thoracic aorta replacement. In our strategy, at the time of replacement of the descending or thoracoabdominal aorta, a cerebrospinal fluid (CSF) drainage catheter is inserted, and motor-evoked potentials are monitored for spinal cord protection. When the amplitudes of the motor-evoked potentials decrease or recover insufficiently, CSF drainage commences. Therefore the cause of the subdural hematoma might be considered to be related to rapid drainage of CSF performed for spinal cord protection. The other patient, who underwent thoracoabdominal aortic replacement for chronic type B aortic dissection, experienced subdural hematoma 2 days postoperatively, although no intracranial lesions were observed on preoperative brain computed tomography. Intracranial aneurysms have been reported as 1 of the arterial lesions related to LDS [7, 8]. In our patient, magnetic resonance or computed tomography angiography for intracranial lesions had not been performed preoperatively; however, we should pay attention to the existence of such intracranial aneurysms.

In 1 particularly interesting case (patient 11, Table 2), aortic dissection occurred from the aortic arch to the abdominal aorta about 6 years after VSRR. The patient had received regular follow-ups and a computed tomographic scan after the initial operation; the maximum diameter of the aortic arch was only 39 mm on a computed tomographic scan taken 1 month before dissection (Fig 3). After this, she underwent total aortic replacement through serial aortic repairs over 1 year. This experience may suggest that a more aggressive strategy be considered to concomitantly repair the aortic arch at the root operation for prevention of future type A aortic dissection, as Augoustides and colleagues [9] advocated. Further follow-up is therefore necessary.

Clinical strategies for aggressive aortic lesions in LDS have yet to be established because there are still few large-scale reports about surgical results and prognoses. However Williams and colleagues [10], who have much experience in aortic operations for patients with LDS, suggested that the threshold for surgical intervention in adult patients with LDS is 4 cm for the aortic root and abdominal aorta and 5 cm for the descending thoracic aorta or for rapid expansion (> 0.5 cm/year) regardless of location. This surgical approach is considered more ag-

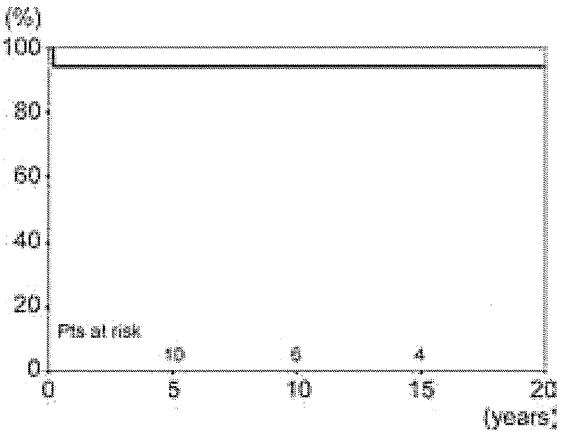

Fig 2. Kaplan-Meier survival curve for all patients (Pts) after first aortic operation.

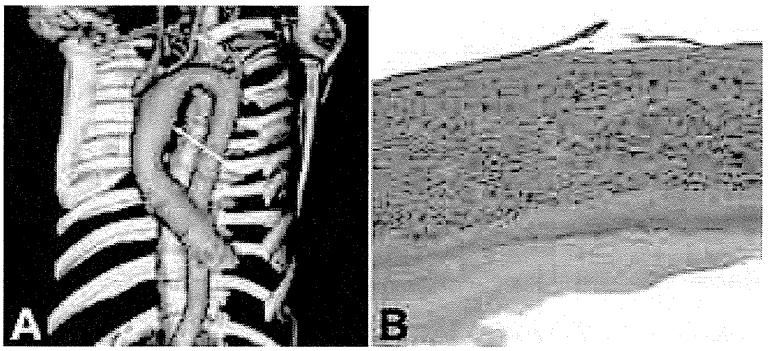

Fig 3. (A) Computed tomographic scan, obtained 1 month before aortic dissection, revealed the maximum diameter of the aortic arch to be 39 mm, with fusiform mild dilatation (arrow). (B) The histopathologic findings of the aortic wall showed diffuse medial degeneration and elastin fragmentation of media (elastica van Gieson stain ×100).

gressive than that for patients with MFS. In our experience, operative results for patients with LDS were satisfactory; moreover, once aortic dissection occurs, most patients need repeated aortic operations [11]. Before this disease was recognized, we had considered surgical indications and management of LDS in the same way as those for MFS. However for the past few years, in which we have recognized the fragile nature of aortic lesions in patients with LDS, we have been adopting a more aggressive strategy for surgical intervention. Therefore we believe that early surgical intervention may improve prognosis by preventing fatal aortic events.

Endovascular treatment should be considered a contraindication in patients with LDS because use of the native aorta as a landing zone carries the risk of potential dilatation. However a recent noteworthy case report describes hybrid therapy, combining open aortic repair and endovascular stent grafting [12].

This study has some limitations. First, our experience with this recently recognized arteriopathy is still limited. Second, this study is retrospective in nature.

In conclusion, we should recognize the aggressive aortic pathologic process in this syndrome, and a clinical management strategy should be established by accumulating further clinical experience.

References

1. Loeys BL, Chen J, Neptune ER, et al. A syndrome of altered cardiovascular craniofacial neurocognitive and skeletal development caused by mutations in TGFBR1 and TGFBR2. Nat Genet 2005;37:275–81.
2. Loeys BL, Schwartze U, Holm T, et al. Aneurysm syndrome caused by mutations in the TGF-beta receptor. N Engl J Med 2006;355:788–98.
3. Van Hemelrijk C, Renard M, Loeys B. The Loeys-Dietz syndrome: an update for the clinician. Curr Opin Cardiol 2010; 25:546–51.
4. Aalberts JJ, van der Berg MP, Bergman JE, et al. The many faces of aggressive aortic pathology: Loeys-Dietz syndrome. Neth Heart J 2008;16:299–304.
5. Maleszewski JJ, Miller DV, Lu J, Dietz HC, Halushka MK. Histopathologic findings in ascending aortas from individuals with Loeys-Dietz syndrome. Am J Surg Pathol 2009;33: 194–201.
6. Patel ND, Arnaoutakis GJ, George TJ, et al. Valve-sparing aortic root replacement in Loeys-Dietz syndrome. Ann Thorac Surg 2011;92:556–61.
7. Levitt MR, Morton RP, Mai JC, Ghodke B, Hallam DK. Endovascular treatment of intracranial aneurysms in Loeys-Dietz syndrome. J Neurointerv Surg 2011 Dec 22. [Epub ahead of print].
8. Rahme RJ, Adel JG, Bendok BR, Bebawy JF, Gupta DK, Batjer HH. Association of intracranial aneurysm and Loeys-Dietz syndrome: case illustration, management, and literature review. Neurosurgery 2011;69:e488–92.
9. Augoustides JG, Plappert T, Bavaria JE. Aortic decision-making in the Loeys-Dietz syndrome: aortic root aneurysm and a normal-caliber ascending aorta and aortic arch. J Thorac Cardiovasc Surg 2009;138:502–3.
10. Williams JA, Loeys BL, Nwakanma LU, et al. Early surgical experience with Loeys-Dietz: a new syndrome of aggressive thoracic aortic aneurysm disease. Ann Thorac Surg 2007;83: S757–63.
11. Williams ML, Wechsler SB, Hughes GC. Two-stage total aortic replacement for Loeys-Dietz syndrome. J Card Surg 2010;25:223–4.
12. Williams JB, McCann RL, Hughes GC. Total aortic replacement in Loeys-Dietz syndrome. J Card Surg 2011;26:304–8.

Cardiology in the Young (2012), 22, 116–119
doi:10.1017/S1047951111001028

Brief Report

Prenatal complex congenital heart disease with Loeys–Dietz syndrome

Yukiko Kawazu,[1] Noboru Inamura,[1] Futoshi Kayatani,[1] Nobuhiko Okamoto,[2] Hiroko Morisaki[3]

[1]Department of Pediatric Cardiology; [2]Department of Medical Genetics, Osaka Medical Center and Research Institute for Maternal and Child Health, Izumi; [3]Department of Bioscience and Genetics, National Cerebral and Cardiovascular Center Research Institute, Suita, Osaka, Japan

Abstract We report an infantile case of Loeys–Dietz syndrome prenatally diagnosed with congenital complex heart disease – double outlet right ventricle and interruption of the aortic arch. The patient also showed prominent dilatation of the main pulmonary artery. Emergency bilateral pulmonary artery banding was performed on the 9th day. However, on the 21st day, the patient died of massive bleeding due to rupture of the right pulmonary artery. Subsequently, a mutation of the TGFBR1 gene was detected. As cardiovascular lesions of Loeys–Dietz syndrome appear early and progress rapidly, the prognosis is generally poor. Patients require periodic examination and early intervention with medical therapy such as Losartan administration and surgical therapy. Early genetic screening is thought to be useful for the prediction of complications as well as vascular disease.

Keywords: Prenatal diagnosis; aneurysm; chromosomal anomaly; connective tissue disorder

Received: 25 January 2011; Accepted: 25 May 2011; First published online: 21 July 2011

LOEYS–DIETZ SYNDROME IS A NEWLY RECOGNISED, rare autosomal dominantly inherited connective tissue disorder caused by heterogeneous mutations in the genes encoding the transforming growth factor beta receptor one or two.[1] This syndrome is characterised by the triad of arterial tortuosity, aneurysm or dissections, hypertelorism, and bifid uvula or cleft palate.[2] Here, we present a patient prenatally diagnosed with complex congenital heart disease and confirmed with Loeys–Dietz syndrome after birth.

Case report

A 31-year-old pregnant woman was referred to our paediatric cardiology unit at the 36th week of gestation because of foetal congenital heart disease and dilatation of the pulmonary artery.

Correspondence to: Y. Kawazu, MD, PhD, 840 Murodo-cho Izumi-city, Osaka 594-1101, Japan. Tel: +81 725 56 1220; Fax: +81 725 56 1858; E-mail: kadoy@mch.pref.osaka.jp

The first foetal echocardiography revealed a huge aneurysm of the main pulmonary artery and complex congenital heart disease – double-outlet right ventricle and interruption of the aortic arch (Fig 1). Detailed multi-planar scanning showed that there was no pulmonary valve stenosis, because of no acceleration in pulmonic flow, and no absent pulmonary valve. Therefore, we suspected a connective tissue disorder, such as Marfan syndrome. The foetus was followed up weekly for foetal decompensation and signs of hydrops until the 39th week of gestation, and an elective caesarean section was then performed. The male infant weighed 2834 grams at birth. After delivery, the infant developed dyspnoea and was intubated for artificial ventilation. Subsequently, a cleft of the soft palate and bifid uvula were noted. To treat the interruption of the aortic arch, we started him on a prostaglandin infusion to maintain patent ductus arteriosus and on nitrogen inhalation to prevent pulmonary blood flow increase. Computed tomography and angiocardiography confirmed the heart

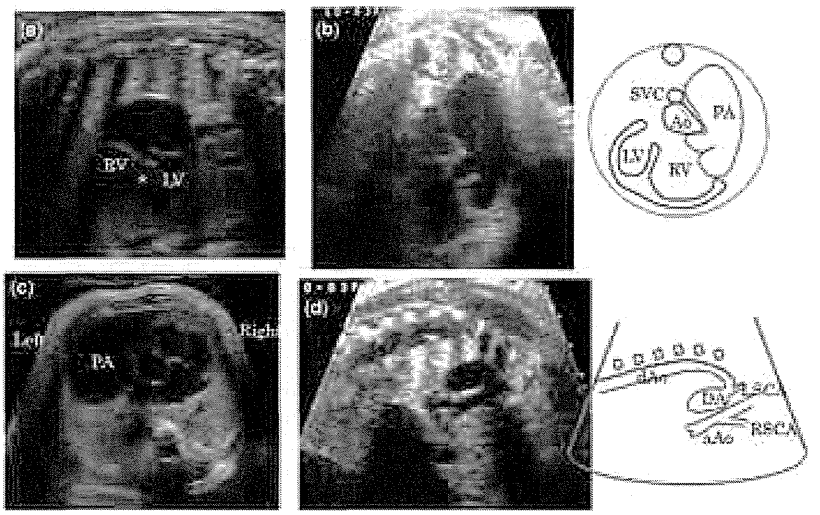

Figure 1.
*Foetal echocardiography shows a large ventricular septal defect (*) of the double-outlet right ventricle (**a**), aneurysmal pulmonary artery (**b, c**), and interruption of the aortic arch (**d**). aAo = ascending aorta; Ao = aorta; DA = ductus arteriosus; dAo = descending aorta; LV = left ventricle; LSCA = left subclavian artery; PA = pulmonary artery; RSCA = right subclavian artery; RV = right ventricle; SVC = supra caval vein.*

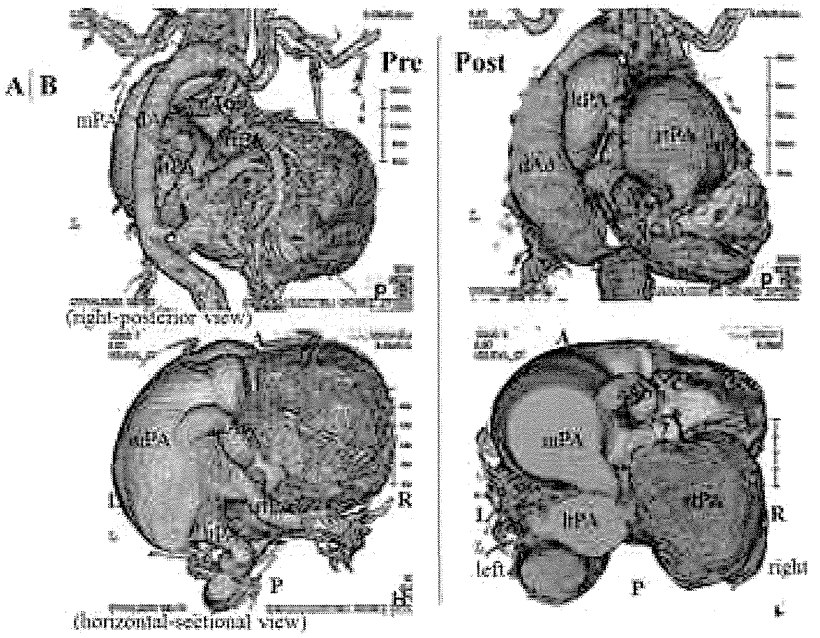

Figure 2.
*Computed tomography (day 0) shows the interruption of the aortic arch and aneurysmal main pulmonary artery before operation (**a**). Computed tomography (day 18) shows progress of the significant expansion of the right and left pulmonary arteries and descending aorta after operation (**b**). A = anterior; aAo = ascending aorta; dAo = descending aorta; L = left; ltpa = left pulmonary artery; P = posterior; mPA = main pulmonary artery; rtPA = right pulmonary artery; R = right.*

disease diagnosed prenatally (Fig 2a). Loeys–Dietz syndrome was strongly suspected because of the presence of cardiovascular lesions, thin skin, and facial appearance. On the 9th day, as the patient had suffered a pulmonary haemorrhage due to pulmonary blood flow increase, emergency bilateral

pulmonary artery banding was performed. However, during surgery, it became apparent that application of normal pulmonary artery banding was impossible because of the very thin condition of the pulmonary artery wall. Therefore, the surgeon performed bilateral banding with the clip, not the usual tape, but the banding was insufficient. This may be a reason why his haemodynamics and respiratory status were not subsequently stable. We again performed computed tomography, which showed a further significant expansion of the right pulmonary artery and descending aorta caused by the pressure of the expanded artery (Fig 2b). Therefore, we started internal use of Losartan. On the 21st day, he developed sudden hypotension and massive bleeding from the thoracic cavity, thought to be caused by right pulmonary rupture, and he died the same day. Subsequently, as the genetic analysis showed p.Thr200Pro (c.598A > C) mutation of the transforming growth factor beta receptor one, he was definitively diagnosed with Loeys–Dietz syndrome. The mutation was *de novo*.

Discussion

Loeys–Dietz syndrome is a recently described connective tissue disorder characterised by aggressive ascending aortic aneurysm and dissection. The clinical features are similar to Marfan syndrome,[3] but this is a more severe syndrome because life-threatening aortic dissection may occur even in early childhood.[4,5] Most patients have the triad of vascular aneurysms, hypertelorism, and bifid or broad uvula/cleft palate associated with variable features. Heterogeneous mutations in the genes encoding for transforming growth factor beta receptors one and two are a consistent finding among affected patients.

In addition, this syndrome shows various cardiovascular manifestations involving not only aortic lesions – such as distortion, aneurysm, and dissections – but also congenital heart diseases.[6] The case described in this report was also complicated with congenital heart disease. The patient's pulmonary artery showed an abnormal expansion because of his heart defect. That is, because he had an interruption of the aortic arch, much more blood than normal flowed through the pulmonary artery and the artery was stressed by "volume overload". Furthermore, the pulmonary artery was stressed by high "pressure overload" because the patient had double-outlet right ventricle and a large ventricular septal defect. It is thought that a pulmonary artery spread for both reasons from the foetal period.

Muramatsu et al[6] reported a case that was complicated with a ventricular septal defect and showed aortic and pulmonary expansion. It is thought that, in the Muramatsu case, the mechanism producing pulmonary artery dilatation was similar to that in the case reported herein. After birth, the patient's pulmonary blood flow increased due to the ventricular septal defect, which led to acute heart failure. He then underwent pulmonary artery banding on the 12th day. After surgery, however, the root of the main pulmonary artery, which was stressed by pressure, had spread in the shape of an aneurysm and intracardiac surgical repair, that is, closure of ventricular septal defect, was performed on the 42nd day. After the operation, the vascular expansion stopped worsening, and in conclusion they recommended early radical operation. However, because our case was a Fontan candidate, he required gradual surgery and radical operation was impossible in early infancy. Therefore, we performed bilateral pulmonary artery banding as a life-saving procedure, but, owing to mural abnormal thinning, the banding was insufficient, and his vascular expansion and thinning progressed, which finally led to explosion and bleeding to death.

In the case reported herein, significant pulmonary expansion from the foetal period led us to suspect a connective tissue disorder such as Marfan syndrome. Viassolo et al[7] reported a similar case in a female patient with Loeys–Dietz syndrome, who showed dilated aortic root from the foetal period. Only aortic dilatation was noted in screening foetal echocardiography at 19 gestational weeks and a connective tissue disease was suspected. She underwent genetic analysis and Loeys–Dietz syndrome was confirmed after birth. At present, the Viassolo case and the one we report herein are the only two cases showing a manifestation of Loeys–Dietz syndrome from the foetal period.

Some cases of Loeys–Dietz syndrome are complicated with congenital heart diseases.[2,6,8] However, those reported hitherto are associated with "simple" congenital heart diseases such as ventricular septal defect, atrial septal defect, patent ductus arteriosus, and aortic bicuspid valve. There is no previous report of Loeys–Dietz syndrome combined with complex congenital heart disease, such as double-outlet right ventricle and interruption of the aortic arch. In such a case, the cardiovascular lesion as an expansion of the great vessels, that is, the aorta or pulmonary artery, may be aggravated during the foetal period. Consequently, the foetus may die in utero. Even if they can be born, their great vessels are continuously or more strongly stressed after birth. Therefore, their arteries expand and finally explode, leading to an early death without undergoing any surgery.

This may be the reason why this is the first reported case of complex heart disease with Loeys–Dietz syndrome.

References

1. Loeys BL, Chen J, Neptune ER, et al. A syndrome of altered cardiovascular, craniofacial, neurocognitive and skeletal development caused by mutations in TGFBR1 or TGFBR2. Nat Genet 2005; 37: 275–281.
2. Loeys BL, Schwarze U, Holm T. Aneurysm syndromes caused by mutations in the TGF-β receptor. N Engl J Med 2006; 355: 788–798.
3. Mizuguchi T, Collod-Beroud G, Akiyama T, et al. Heterozygous TGFBR2 mutations in Marfan syndrome. Nat Genet 2004; 36: 855–860.
4. Yamawaki T, Nagaoka K, Morishige K, et al. Familial thoracic aortic aneurysm and dissection associated with Marfan-related gene mutations: case report of a family with two gene mutations. Intern Med 2009; 48: 555–558.
5. Akutsu K, Morisaki H, Okajima T, et al. Genetic analysis of young adult patients with aortic disease not fulfilling the diagnostic criteria for Marfan syndrome. Circ J 2010; 74: 990–997.
6. Muramatsu Y, Kosho T, Magota M, et al. Progressive aortic root and pulmonary artery aneurysms in a neonate with Loeys–Dietz syndrome type 1B. Am J Med Genet A 2010; 152A: 417–421.
7. Viassolo V, Lituania M, Marasini M, et al. Fetal aortic root dilation: a prenatal feature of the Loeys–Dietz syndrome. Prenat Diagn 2006; 26: 1081–1083.
8. Watanabe Y, Sakai H, Nishimura A, et al. Paternal somatic mosaicism of a TGFBR2 mutation transmitting to an affected son with Loeys–Dietz syndrome. Am J Med Genet A 2008; 146A: 3070–3074.

Acta Oto-Laryngologica, 2013; 133: 345–351

informa
healthcare

ORIGINAL ARTICLE

Genetic analysis of *PAX3* for diagnosis of Waardenburg syndrome type I

TATSUO MATSUNAGA[1], HIDEKI MUTAI[1], KAZUNORI NAMBA[1], NORIKO MORITA[2] & SAWAKO MASUDA[3]

[1]*Department of Otolaryngology, Laboratory of Auditory Disorders, National Institute of Sensory Organs, National Tokyo Medical Center, Tokyo,* [2]*Department of Otolaryngology, Teikyo University School of Medicine, Tokyo and* [3]*Department of Otorhinolaryngology, Institute for Clinical Research, National Mie Hospital, Tsu, Japan*

Abstract

Conclusion: PAX3 genetic analysis increased the diagnostic accuracy for Waardenburg syndrome type I (WS1). Analysis of the three-dimensional (3D) structure of PAX3 helped verify the pathogenicity of a missense mutation, and multiple ligation-dependent probe amplification (MLPA) analysis of *PAX3* increased the sensitivity of genetic diagnosis in patients with WS1. *Objectives:* Clinical diagnosis of WS1 is often difficult in individual patients with isolated, mild, or non-specific symptoms. The objective of the present study was to facilitate the accurate diagnosis of WS1 through genetic analysis of *PAX3* and to expand the spectrum of known *PAX3* mutations. *Methods:* In two Japanese families with WS1, we conducted a clinical evaluation of symptoms and genetic analysis, which involved direct sequencing, MLPA analysis, quantitative PCR of *PAX3*, and analysis of the predicted 3D structure of PAX3. The normal-hearing control group comprised 92 subjects who had normal hearing according to pure tone audiometry. *Results:* In one family, direct sequencing of *PAX3* identified a heterozygous mutation, p. I59F. Analysis of PAX3 3D structures indicated that this mutation distorted the DNA-binding site of PAX3. In the other family, MLPA analysis and subsequent quantitative PCR detected a large, heterozygous deletion spanning 1759–2554 kb that eliminated 12–18 genes including a whole *PAX3* gene.

Keywords: *Mutation, MLPA, clinical diagnosis, hearing loss, dystopia canthorum, pigmentary disorder*

Introduction

Waardenburg syndrome (WS) is a hereditary auditory pigmentary disorder that is responsible for 1–3% of congenital deafness cases [1]. WS is classified into four types based on symptoms other than the auditory and pigmentary disorder. Type I WS (WS1) includes dystopia canthorum, and this feature distinguishes WS1 from type II WS. Type III WS is similar to WS1 but is associated with musculoskeletal anomalies of the upper limbs. Type IV WS is similar to type I but is associated with Hirschsprung disease. Diagnostic criteria for WS1 have been proposed [2]. The clinical features of WS1 demonstrate incomplete penetrance and highly varied expression [3,4], which makes diagnosis in individual patients challenging. For example, WS1 patients may present only one isolated symptom. Diagnosis of high nasal root and medial eyebrow flare can be difficult when they are mild. Hearing loss and early graying are relatively common in the general population and are not specific to WS1. Thus, the accuracy of WS1 diagnosis needs to be improved by the use of additional diagnostic procedures.

It is reported that more than 90% of patients with WS1 harbor point mutations in *PAX3* [5], and an additional 6% of WS1 patients harbor partial or complete *PAX3* deletions [6]. This high frequency of *PAX3* mutation in WS1 suggests that clinical diagnosis of WS1 could be facilitated by *PAX3* genetic analysis. To date, more than 80 *PAX3*

Correspondence: Tatsuo Matsunaga, Department of Otolaryngology, Laboratory of Auditory Disorders, National Institute of Sensory Organs, National Tokyo Medical Center, 2-5-1 Higashigaoka, Meguro, Tokyo, 152-8902, Japan. Tel: +81 3 3411 0111. Fax: +81 3 3412 9811. E-mail: matsunagatatsuo@kankakuki.go.jp

This study was presented at the annual meeting of the Collegium Oto-Rhino-Laryngologicum Amicitiae Sacrum, Rome, August 28, 2012.

(Received 19 September 2012; accepted 20 October 2012)

ISSN 0001-6489 print/ISSN 1651-2251 online
DOI: 10.3109/00016489.2012.744470

mutations are reported to be associated with WS1 [5]. A de novo paracentric inversion on chromosome 2 in a Japanese child with WS1 provided a clue for identification of *PAX3* in the distal part of chromosome 2 [7]. However, only a few *PAX3* mutations including the chromosomal inversion have been reported in Japanese patients with WS1 since then [8,9].

In the present study, we conducted *PAX3* genetic analysis to facilitate diagnosis of WS1 in two Japanese families. In one family, to verify the pathogenicity of an identified missense mutation, we analyzed the effect of the mutation on the three-dimensional (3D) structure of PAX3. In the other family, no mutations were identified by direct sequencing, so multiple ligation-dependent probe amplification (MLPA) analysis was used to search for large deletions in *PAX3* and thereby increase the sensitivity of genetic diagnosis.

Material and methods

Patients and control subjects

Two Japanese families with WS1 were included in the study. The diagnosis of WS1 was based on criteria proposed by the Waardenburg Consortium [2]. The normal-hearing controls comprised 92 subjects who had normal hearing according to pure tone audiometry. This study was approved by the institutional ethics review board at the National Tokyo Medical Center. Written informed consent was obtained from all subjects included in the study or from their parents.

Clinical evaluation

A comprehensive clinical history was taken from subjects who were examined at our hospitals or from their parents. During physical examination, special attention was given to the color of the skin, hair, and iris, and to other anomalies such as dystopia canthorum, medial eyebrow flare, limb abnormalities, and Hirschsprung disease. After otoscopic examination, behavioral audiometric testing was performed. The test protocol was selected according to the developmental age of the subject (conditioned orientation response audiometry, play audiometry, or conventional audiometric testing, from 125 to 8000 Hz), and testing was performed using a diagnostic audiometer in a soundproof room. Auditory brainstem response (ABR) and otoacoustic emission were also evaluated in some subjects.

Direct sequencing

Genomic DNA from the subjects was extracted from peripheral blood leukocytes using the Gentra Puregene® Blood kit (QIAGEN, Hamburg, Germany). Mutation screening of *PAX3* was performed by bidirectional sequencing of each exon (exons 1–11) together with the flanking intronic regions using an ABI 3730 Genetic Analyzer (Applied Biosystems, Foster City, CA, USA). Primer sequences for *PAX3* are listed in Table I. Mutation nomenclature is based on the genomic DNA sequence of [GenBank accession no. NG_011632.1], with the A of the translation initiation codon considered as +1. Nucleotide conservation between mammalian species was evaluated using ClustalW (http://www.ebi.ac.uk/Tools/msa/clustalw2/). PolyPhen-2 software (http://genetics.bwh.harvard.edu/pph2/) was used to predict the functional consequence(s) of each amino acid substitution.

MLPA

MLPA analysis was performed using an MLPA kit targeting *PAX3*, *MITF*, and *SOX10* (SALSA MLPA Kit P186-B1, MRC-Holland, Amsterdam, The Netherlands) according to the manufacturer's protocol. Exon-specific MLPA probes for exons 1–9 of *PAX3* and control probes were hybridized to genomic DNA from the subjects and normal controls and ligated with fluorescently labeled primers. A PCR reaction was then performed to amplify the hybridized probes. The amplified probes were fractionated on an ABI3130xl Genetic Analyzer (Applied Biosystems) and the peak patterns were evaluated using GeneMapper (Applied Biosystems).

Real-time PCR

To determine the length of each deleted genomic region, 100 ng of genomic DNA from the subjects and a normal control were subjected to quantitative PCR (Prism 7000, Applied Biosystems) using Power SYBR® Green Master Mix (Life Technologies, Carlsbad, CA, USA) and 12 sets of primers designed to amplify sequence-tagged sites on chromosome 2 (GenBank accession nos: RH46518, RH30035, RH66441, GDB603632, 1988, RH24952, RH47422, RH65573, RH26526, RH35885, RH16314, and RH92249).

Homology modeling of the PAX3 paired domain

The DNA-binding site of the paired domain of PAX3 was modeled using SWISS-MODEL [10] with the crystal structure of the PAX5 paired domain-DNA complex (PDB ID:1PDN_chain C) as the template because PAX3 and PAX5 are functionally and structurally similar [11]. The amino acid

Table I. Primer sequences for *PAX3*.

Exon 1	Forward	5′-TGTAAAACGACGGCCAGTAGAGCAGCGCGCTCCATTTG-3′
	Reverse	5′-CAGGAAACAGCTATGACCGCTCGCCGTGGCTCTCTGA-3′
Exon 2	Forward	5′-TGTAAAACGACGGCCAGTAAGAAGTGTCCAGGGCGCGT-3′
	Reverse	5′-CAGGAAACAGCTATGACCGGTCTGGGTCTGGGAGTCCG-3′
Exon 3	Forward	5′-TGTAAAACGACGGCCAGTTAAACGCTCTGCCTCCGCCT-3′
	Reverse	5′-CAGGAAACAGCTATGACCGGGATGTGTTCTGGTCTGCCC-3′
Exon 4	Forward	5′-TGTAAAACGACGGCCAGTAATGGCAACAGAGTGAGAGCTTCC-3′
	Reverse	5′-CAGGAAACAGCTATGACCAGGAGACACCCGCGAGCAGT-3′
Exon 5	Forward	5′-TGTAAAACGACGGCCAGTGGTGCCAGCACTCTAAGAACCCA-3′
	Reverse	5′-CAGGAAACAGCTATGACCGGTGATCTGACGGCAGCCAA-3′
Exon 6	Forward	5′-TGTAAAACGACGGCCAGTTGCATCCCTAGTAAAGGGCCA-3′
	Reverse	5′-CAGGAAACAGCTATGACCGGTGTCCATGGAAGACATTGGG-3′
Exon 7	Forward	5′-AACTATTATTTCATCAGTGAAATC-3′
	Reverse	5′-ATTCACTTGTATAAAATATCCACC-3′
Exon 8	Forward	5′-TGTAAAACGACGGCCAGTTGAAGCCAGTAGGAAGGGTGGA-3′
	Reverse	5′-CAGGAAACAGCTATGACCTGCAGGTTAAGAAACGCAGTTTGA-3′
Exon 9a	Forward	5′-TGTAAAACGACGGCCAGTTTGATACCGGCATGTGTGGC-3′
	Reverse	5′-CAGGAAACAGCTATGACCTGCAGTCAGATGTTATCGTCGGG-3′
Exon 9b	Forward	5′-TGTAAAACGACGGCCAGTCACAACTTTGTGTCCCTGGGATT-3′
	Reverse	5′-CAGGAAACAGCTATGACCGGGACTCCTGACCAACCACG-3′
Exon 10–11	Forward	5′-TGTAAAACGACGGCCAGTGCAAATGGAATGTTCTAGCTCCTCG-3′
	Reverse	5′-CAGGAAACAGCTATGACCGGTCAGCTCCAGGATCATATGGG-3′

sequences of the PAX3 and PAX5 paired domains were 79% homologous. The predicted PAX3 structure and the p.I59F mutation structure were superimposed on the backbone atoms of the PAX5 paired domain-DNA complex and displayed using the extensible visualization system, UCSF Chimera [12].

Results

In family 1, the proband, a 9-month-old male, was the first child of unrelated Japanese parents. Abnormal responses were found upon newborn hearing screening in the left ear, and left hearing loss was diagnosed by ABR. On physical examination, dystopia canthorum was noted, with a W-index of 2.77. The patient's mother also had dystopia canthorum, with a W-index of 2.68. She also had a history of early graying that started at age 16 years. She had not been diagnosed with WS1. According to the parents, 10 members of this family, including the proband and the mother, showed clinical features consistent with WS1 (Figure 1). ABR performed in the proband

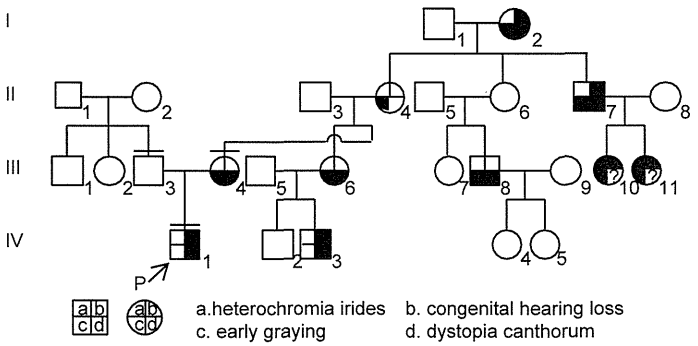

Figure 1. Pedigree of family 1. The proband is indicated by an arrow. The individuals we examined personally are indicated by a bar over the symbol. Phenotypes observed in this family are indicated symbolically as detailed below the pedigree.

revealed normal hearing in the right ear and no responses to 105 dB click stimuli in the left ear. Computed tomography (CT) of the temporal bone showed normal structures in the inner, middle, and outer ears.

Genetic analysis of *PAX3* was conducted in this family, and direct sequencing of *PAX3* revealed a heterozygous mutation, c.175A>T, in the proband and his mother. This mutation resulted in a missense mutation, p.I59F (Figure 2A). The proband's father did not harbor this mutation. p.I59F is located within exon 2 and is part of the paired domain of *PAX3*, which is a critical region for interaction between transcription factors and target DNA (Figure 2B). A multiple alignment of *PAX3* orthologs at this region demonstrated that I59 was evolutionarily conserved among various species (Figure 2C). The p.I59F mutation was not identified in any of the 184 alleles from the normal control subjects. This mutation was predicted to be 'probably damaging' according to PolyPhen-2 software.

The predicted 3D structures of the paired domain of the PAX3-DNA complex indicated that the PAX3 paired domain binds to the corresponding DNA (white double helixes) via hydrogen bonds (pink lines) at the N-terminal of α-helix1 (H1), α-helix2 (H2), and α-helix3 (H3) (indicated in blue; Figure 3A). I59 is located in the middle of H1, H2, and H3 and is surrounded by hydrophobic residues (green) protruding from H1, H2, and H3. Because the van der Waals radius of phenylalanine (Figure 3C; white arrows) is larger than that of isoleucine (Figure 3B, white arrowheads), F59 repels the surrounding hydrophobic residues by van der Waals forces and increases the distance between F59 and the surrounding hydrophobic residues, resulting in structural distortion of the DNA-binding site of PAX3. Since this site is precisely shaped for maximal binding to the corresponding DNA, this mutation is likely to reduce the binding ability of the paired domain of PAX3 and cause WSI. A mutational search found the same mutation in another Japanese family [8].

In family 2, the proband, a female aged 4 years and 4 months, was the first child of unrelated Japanese parents. Abnormal responses were found upon newborn hearing screening in the right ear, and right hearing loss was diagnosed by ABR. On physical examination, dystopia canthorum, medial eyebrow flare, and a white forelock were noted. She was admitted to hospital suffering from ketotic hypoglycemia of unknown cause when aged 4 years. Her mother presented with heterochromia iridis, dystopia canthorum, and medial eyebrow flare, and her grandmother presented with early graying that started at around 20 years of age, dystopia canthorum, and

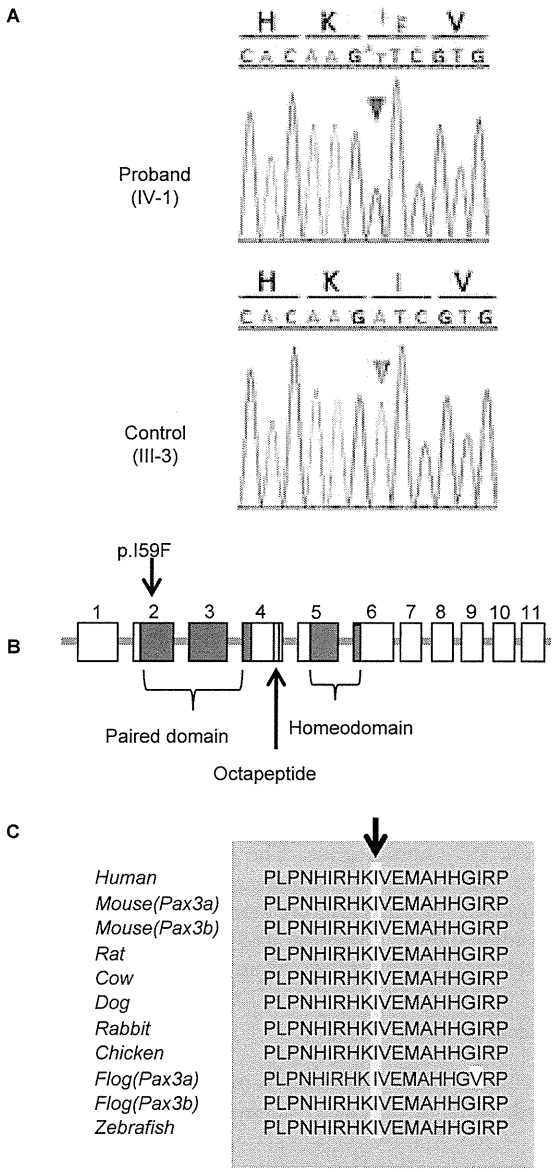

Figure 2. The p.I59F mutation of *PAX3* detected in family 1. (A) Sequence chromatogram for the proband and unaffected control. A heterozygous A to T transversion (red arrowhead) that changes codon 59 from ATC, encoding isoleucine (I), to TTC, encoding phenylalanine (F), was detected in the proband but not in the control (green arrowhead). (B) Localization of the p.I59F mutation and functional domains of PAX3. (C) A multiple alignment of PAX3 orthologs. Regions of amino acid sequence identity are shaded gray. The position of I59 is indicated by an arrow and shaded yellow.

medial eyebrow flare. According to the grandmother, the father of the grandmother also had dystopia canthorum and medial eyebrow flare. The pedigree of family 2 is shown in Figure 4. The grandmother

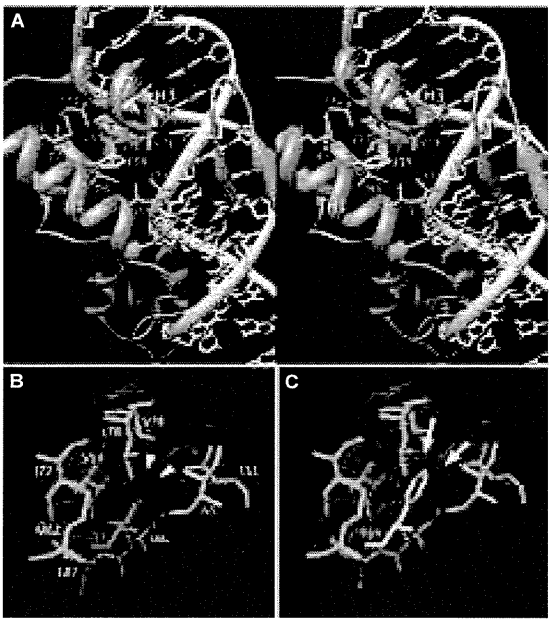

Figure 3. The predicted structure of the PAX3 paired domain-DNA complex. (A) The stereo view indicates that the mutated residue was surrounded by hydrophobic residues (green) protruding from H1, H2, and H3 of the paired domain (blue), which binds to DNA (white, sugar; blue, nitrogen; red, oxygen). The pink lines indicate hydrogen bonds. Magenta and yellow residues indicate I59 and F59, respectively. (B, C) The colored spheres indicate the van der Waals surface boundaries, the radius of the hydrophobic residues is shown in green, I59 is shown in magenta and is also indicated by arrowheads, and F59 is shown in yellow and is also indicated by arrows.

and her father had never been diagnosed with WS1. Pure tone audiometry of the proband showed severe hearing loss in the right ear and normal hearing in the left ear. The results of ABR and distortion product otoacoustic emissions in the proband were compatible with those obtained for pure tone audiometry.

Because direct sequencing of *PAX3* in the proband and her grandmother revealed no mutations, we conducted MLPA analysis to search for a large deletion of *PAX3*, and found that the copy number of all tested exons (exons 1–9) of *PAX3* was half that of the number of other chromosomal regions in both subjects (Figure 5A). In control subjects, all tested exons of *PAX3* showed the same copy number as the other chromosomal regions (Figure 5B). To determine the size of the deleted region, quantitative PCR was performed at 12 sequence-tagged sites on chromosome 2q36, which includes *PAX3*. In the proband, copy numbers at nine sites in the middle of the tested region (white arrows) were half that of those examined in normal controls, but the copy numbers at three of the sites near the 5' and 3' ends of the tested region (black arrows) were identical to those examined in normal controls (Figure 6). This result demonstrated that the chromosomal region spanning 1759–2554 kb at 2q36, which includes the whole *PAX3* gene, was deleted in one of the alleles of the proband. The same results were detected in the grandmother. A search for the deleted region revealed that this region contained between 12 and 18 genes, including *PAX3*.

Discussion

The heterozygous missense mutation, p.I59F, was identified in family 1. The pathogenicity of a novel or rare missense mutation in the causative gene is not necessarily verified even when the mutation is absent from a large number of normal controls, when the residue is evolutionary conserved among different species, or if the mutation is associated with the phenotype within a family, because an identified

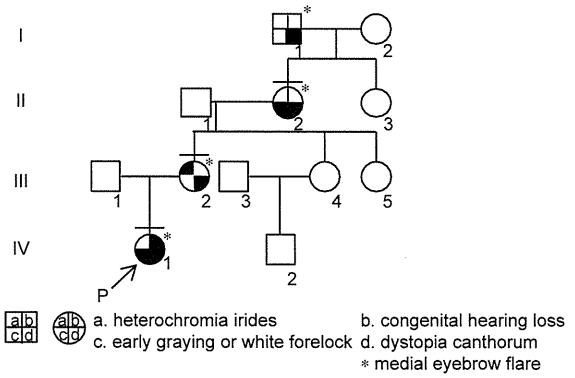

Figure 4. Pedigree of family 2. The proband is indicated by an arrow. The individuals we examined personally are indicated by a bar over the symbol. Phenotypes observed in this family are indicated symbolically, as detailed below the pedigree.

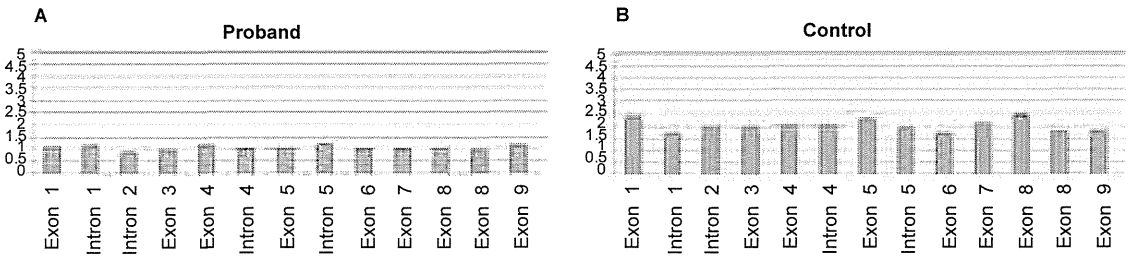

Figure 5. Results of MLPA analysis of *PAX3* in family 2. (A, B) Relative ratios of DNA quantity in each exon compared with that in the control region are shown for the proband (A) and control (B).

missense mutation may be a rare normal variant. Thus, the pathogenicity of such mutations needs to be verified by detection of the same mutation in multiple families with the same phenotype or by functional analysis. The functional consequences of a few *PAX3* mutations have been tested and reduced DNA-binding properties have been reported [13–15]. The p.I59F mutation was reported in a Japanese family [8], but functional analysis has not been conducted. We analyzed the predicted 3D structures of the paired domain of the PAX3-DNA complex and showed that this mutation was likely to distort the structure of the DNA-binding site of PAX3 and lead to functional impairment. This result substantially supports the hypothesis that the p.I59F mutation is pathogenic, although it is based on a theoretical prediction rather than functional experiments.

In family 2, the distinct phenotypes of the proband, the proband's mother, and the proband's grandmother were congenital unilateral hearing loss, heterochromia iridis, and early graying, respectively. Because of these differences, they were not aware of the hereditary nature of the symptoms. Identification of the *PAX3* mutation in the proband and the proband's grandmother led to an accurate diagnosis of WS1 and facilitated understanding of the symptoms. In this family, direct sequencing of *PAX3* did not detect any mutations, but MLPA analysis detected a large heterozygous deletion. Furthermore, quantitative PCR analysis revealed that the deleted region spanned 1759–2554 kb and included 12–18 genes. Large deletions of *PAX3* in patients with WS1 have been reported in several families [6,16–18]. To our knowledge, however, this is the largest deletion identified in patients with WS1 and has, therefore, expanded the spectrum of *PAX3* mutations. There is no reported correlation between the nature of the mutation (deleted vs truncated or missense) or

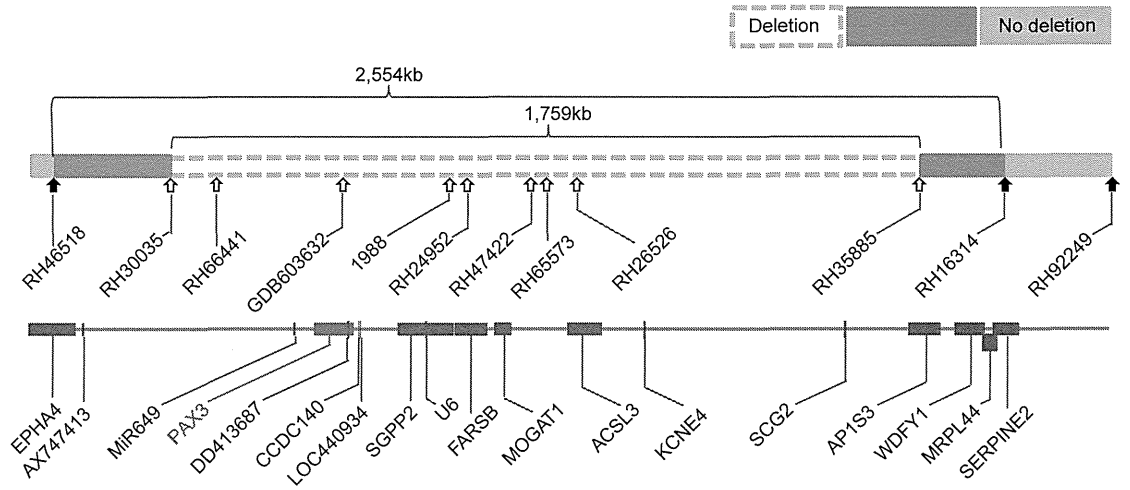

Figure 6. Genetic map showing the estimated location of the *PAX3* deletion together with the regions surrounding *PAX3*. Sites examined by quantitative PCR are indicated by arrows. Blank and white arrows indicate that the quantities of DNA at these sites are half or identical to the quantities of DNA at the corresponding sites in the control, respectively. The 5′ and 3′ ends of the deletion are located within the blue regions flanking the white region, designated as 'deletion,' and flanked by the green regions, designated as 'no deletion.' All genes mapped within this region, including *PAX3*, are shown in the lower map.

its location in *PAX3*, and the severity of the WS1 phenotype [19,20]. Similarly, no evidence of such a correlation was found in the data presented in this study.

In the present study, *PAX3* genetic diagnosis contributed to the accurate diagnosis of WS1. Such diagnosis could help provide genetic counseling to patients with isolated or few phenotypic symptoms, those with mild phenotypes or few first-degree relatives, or those who have yet to develop any symptoms. In addition, analysis of the predicted 3D structure of PAX3 facilitated the verification of pathogenicity of a missense mutation, and MLPA analysis increased the sensitivity of genetic diagnosis of WS1.

Acknowledgments

We thank the families that participated in this study. This study was supported by a Grant-in-Aid for Clinical Research from the National Hospital Organization, and by a Health and Labour Sciences Research Grants for Research on Rare and Intractable Diseases from the Ministry of Health, Labour and Welfare of Japan.

Declaration of interest: The authors report no conflicts of interest. The authors alone are responsible for the content and writing of the paper.

References

[1] Read AP, Newton VE. Waardenburg syndrome. J Med Genet 1997;34:656–65.
[2] Farrer LA, Grundfast KM, Amos J, Arnos KS, Asher JH Jr, Beighton P, et al. Waardenburg syndrome (WS) type I is caused by defects at multiple loci, one of which is near ALPP on chromosome 2: first report of the WS consortium. Am J Hum Genet 1992;50:902–13.
[3] Liu XZ, Newton VE, Read AP. Waardenburg syndrome type II: phenotypic findings and diagnostic criteria. Am J Med Genet 1995;55:95–100.
[4] Pardono E, van Bever Y, van den Ende J, Havrenne PC, Iughetti P, Maestrelli SR, et al. Waardenburg syndrome: clinical differentiation between types I and II. Am J Med Genet A 2003;117A:223–35.
[5] Pingault V, Ente D, Dastot-Le Moal F, Goossens M, Marlin S, Bondurand N. Review and update of mutations causing Waardenburg syndrome. Hum Mutat 2010;31:391–406.
[6] Milunsky JM, Maher TA, Ito M, Milunsky A. The value of MLPA in Waardenburg syndrome. Genet Test 2007;11:179–82.
[7] Ishikiriyama S, Tonoki H, Shibuya Y, Chin S, Harada N, Abe K, et al. Waardenburg syndrome type I in a child with de novo inversion (2)(q35q37.3). Am J Med Genet 1989;33:505–7.
[8] Soejima H, Fujimoto M, Tsukamoto K, Matsumoto N, Yoshiura KI, Fukushima Y, et al. Three novel PAX3 mutations observed in patients with Waardenburg syndrome type 1. Hum Mutat 1997;9:177–80.
[9] Kashima T, Akiyama H, Kishi S. Asymmetric severity of diabetic retinopathy in Waardenburg syndrome. Clin Ophthalmol 2011;5:1717–20.
[10] Kiefer F, Arnold K, Kunzli M, Bordoli L, Schwede T. The SWISS-MODEL Repository and associated resources. Nucleic Acids Res 2009;37:D387–92.
[11] Xu W, Rould MA, Jun S, Desplan C, Pabo CO. Crystal structure of a paired domain-DNA complex at 2.5 A resolution reveals structural basis for Pax developmental mutations. Cell 1995;80:639–50.
[12] Pettersen EF, Goddard TD, Huang CC, Couch GS, Greenblatt DM, Meng EC, et al. UCSF Chimera – a visualization system for exploratory research and analysis. J Comput Chem 2004;25:1605–12.
[13] Chalepakis G, Goulding M, Read A, Strachan T, Gruss P. Molecular basis of splotch and Waardenburg Pax-3-mutations. Proc Natl Acad Sci USA 1994;91:3685–9.
[14] Corry GN, Underhill DA. Pax3 target gene recognition occurs through distinct modes that are differentially affected by disease-associated mutations. Pigment Cell Res 2005;18:427–38.
[15] Fortin AS, Underhill DA, Gros P. Reciprocal effect of Waardenburg syndrome mutations on DNA binding by the Pax-3 paired domain and homeodomain. Hum Mol Genet 1997;6:1781–90.
[16] Baldwin CT, Lipsky NR, Hoth CF, Cohen T, Mamuya W, Milunsky A. Mutations in PAX3 associated with Waardenburg syndrome type I. Hum Mutat 1994;3:205–11.
[17] Tassabehji M, Newton VE, Leverton K, Turnbull K, Seemanova E, Kunze J, et al. PAX3 gene structure and mutations: close analogies between Waardenburg syndrome and the Splotch mouse. Hum Mol Genet 1994;3:1069–74.
[18] Wang J, Li S, Xiao X, Wang P, Guo X, Zhang Q. PAX3 mutations and clinical characteristics in Chinese patients with Waardenburg syndrome type 1. Mol Vis 2010;16:1146–53.
[19] Baldwin CT, Hoth CF, Macina RA, Milunsky A. Mutations in PAX3 that cause Waardenburg syndrome type I: ten new mutations and review of the literature. Am J Med Genet 1995;58:115–22.
[20] Tassabehji M, Newton VE, Liu XZ, Brady A, Donnai D, Krajewska-Walasek M, et al. The mutational spectrum in Waardenburg syndrome. Hum Mol Genet 1995;4:2131–7.

CLINICAL REPORT

AMERICAN JOURNAL OF medical genetics PART A

Heterozygous Tandem Duplication Within the *PTCH1* Gene Results in Nevoid Basal Cell Carcinoma Syndrome

Rika Kosaki,[1] Kazuaki Nagao,[2] Kohzoh Kameyama,[2] Maiko Suzuki,[2] Katsunori Fujii,[3] and Toshiyuki Miyashita[2]*

[1]Division of Medical Genetics, National Center for Child Health and Development, Tokyo, Japan

[2]Department of Molecular Genetics, Kitasato University Graduate School of Medical Sciences, Sagamihara, Japan

[3]Department of Pediatrics, Chiba University Graduate School of Medicine, Chiba, Japan

Manuscript Received: 10 November 2011; Manuscript Accepted: 18 March 2012

Nevoid basal cell carcinoma syndrome (NBCCS) is an autosomal dominant disorder characterized by developmental defects and tumorigenesis. The gene responsible for NBCCS is *PTCH1*. Using multiplex ligation-dependent probe amplification, we identified a heterozygous tandem duplication within the *PTCH1* gene in a 14-year-old girl with typical NBCCS. We have sequenced the chromosomal breakpoint and determined the duplication as tandem in orientation and 18,814 bp in size. The fusion occurred between non-repetitive elements with an overlap of three nucleotides. The duplicated segment began at exon 10 and ended at intron 17. Subsequent analysis of cDNA from the patient showed the expression of mutant mRNA species containing a duplicated segment spanning exons 11–17, resulting in a frameshift and premature stop codon. This is the first reported case of NBCCS due to a tandem multiexon duplication of *PTCH1* representing a novel mechanism leading to the NBCCS phenotype, and highlights the importance of copy number analysis as an adjunct to exon sequencing in identifying infrequent mutational events in *PTCH1*.

Key words: nevoid basal cell carcinoma syndrome; *PTCH1*; tandem duplication

How to Cite this Article:
Kosaki R, Nagao K, Kameyama K, Suzuki M, Fujii K, Miyashita T. 2012. Heterozygous tandem duplication within the *PTCH1* gene results in nevoid basal cell carcinoma syndrome.
Am J Med Genet Part A 158A:1724–1728.

INTRODUCTION

Nevoid basal cell carcinoma syndrome (NBCCS) (OMIM 109400), also known as Gorlin syndrome, is an autosomal dominant disorder characterized by developmental defects including bifid ribs, palmar or plantar pits and tumorigenesis such as the development of basal cell carcinoma, medulloblastoma, or keratocystic odontogenic tumor (KCOT) (formerly known as odontogenic keratocysts) [Gorlin, 1987]. The gene responsible for NBCCS is the human homologue of the *Drosophila patched* gene, *PTCH1* [Hahn et al., 1996; Johnson et al., 1996]. The human *PTCH1* gene contains 23 coding exons spanning approximately 70 kb and encodes a protein of 1447 amino-acid residues containing 12 transmembrane-spanning domains and two large extracellular loops [Johnson et al., 1996]. To date, we have analyzed 42 NBCCS families. Nine of the families (21%) did not harbor *PTCH1* mutations detectable by PCR-based direct sequencing of the exons. Five of these mutation-negative families could be explained by large deletions involving complete loss of one copy of *PTCH1* [Fujii et al., 2007; Nagao et al., 2011].

Here we report on a novel mutation involving duplication of eight exons detected in one of the four remaining families. This is the first report of a multiexon duplication event in NBCCS.

CLINICAL REPORT

The propositus was a Japanese girl who was referred to our genetic clinic at the age of 14 years for evaluation. The parents were non-consanguineous and phenotypically normal. The propositus was a second child and had been delivered vaginally at 38 weeks of gestation. Her birth weight was 3,676 g (+1.8 SD), her crown-to-heel

Grant sponsor: Ministry of Health, Labour and Welfare; Grant sponsor: Ministry of Education, Culture, Sports, Science and Technology 20591261.
*Correspondence to:
Toshiyuki Miyashita, M.D., Ph.D., Department of Molecular Genetics, Kitasato University School of Medicine, 1-15-1 Kitasato, Minami-ku, Sagamihara 252-0374, Japan. E-mail: tmiyashi@med.kitasato-u.ac.jp
Article first published online in Wiley Online Library (wileyonlinelibrary.com): 7 June 2012
DOI 10.1002/ajmg.a.35412

length was 54 cm (+2.7 SD), and her head circumference was 36 cm (+1.0 SD).

Her development was normal. She gained head control at the age of 3 months, sat at the age of 6 months, and walked alone at the age of 14 months. At the age of 10 years, she developed bilateral maxillary and mandibular cysts, which were surgically enucleated. A histological examination of the cystic linings showed the presence of KCOT, prompting a clinical diagnosis of NBCCS. The presence of numerous pits over her palms and soles and lamellar calcification on the falx detected using cranial computed tomography was compatible with the diagnosis. Two additional surgeries were subsequently performed to remove KCOTs. Vertebral defects, including fusion of the vertebral bodies or hemivertebrae, were not noted on a skeletal survey.

At the age of 15 years and 6 months, she weighed 54.8 kg (+0.3 SD) and was 168.5 cm tall (+2.1 SD). Physical examination identified macrocephaly, ocular hypertelorism and several pits over her palms and soles. Ten patches of basal cell nevi were noted on her back. Radiological examination did not show rib or vertebrate anomalies. Her parents did not have NBCCS manifestations.

METHODS

DNA and RNA Extraction

All experiments described below were approved by the ethics committee at Kitasato University. DNA was extracted from peripheral blood lymphocytes using a QIAamp DNA blood midi kit (QIAGEN, Germantown, MD) and RNA from established lymphoblastoid cell lines derived from the patient and a healthy control using a QIAamp RNA Blood Mini Kit (QIAGEN) and cDNA prepared using standard laboratory protocols. Lymphoblastoid cell lines were grown in the presence or absence of puromycin (100 μg/ml) for 6 hr prior to RNA extraction.

PCR and Sequence Analysis

The complete coding region of the *PTCH1* gene, including all splice junctions, was amplified from constitutional DNA as described previously [Fujii et al., 2003]. Amplified products were gel-purified using a QIAEX II gel extraction kit (QIAGEN) and cycle sequenced with a BigDye Terminator v3.1 Cycle Sequencing Kit (Applied Biosystems, Carlsbad, CA) in both directions. The sequence was analyzed on a 3130 Genetic Analyzer (Applied Biosystems). The duplication junction was determined by direct sequencing for the PCR product obtained with a forward primer P1 (5′-TGCGAAGCTCAGCTTCTGTGC-3′) hybridizing to intron 16 and a reverse primer P2 (5′-TACTGGGTCAGACTGAGGAA-3′) hybridizing to intron 11. The mutant mRNA was sequenced for the RT-PCR product obtained with a forward primer P3 (5′-TTACGACCTACACAGGAGTT-3′) hybridizing to exon 15 and a reverse primer P4 (5′-ATCCAGTCTCCTGTCCTCGC-3′) hybridizing to exon13.

MLPA Analysis

The multiplex ligation-dependent probe amplification (MLPA)-Gorlin kit was obtained from MRC-Holland (Amsterdam, The Netherlands). MLPA reactions were performed according to the manufacturer's instructions. Products were analyzed using a 3130 Genetic Analyzer (Applied Biosystems) and GeneMapper software (Applied Biosystems).

Southern Blotting

Southern blotting was performed using standard laboratory protocols. The probe DNA hybridizing with the intron 16 sequence was amplified by PCR with a forward primer P5 (5′-CTTGGAATCAGAGTGGCTGC-3′) and a reverse primer P6 (5′-TCTGGCCCAATCCCATTTGT-3′) and radiolabeled with α-^{32}P-dATP during the PCR procedure.

RESULTS

In this case, direct sequencing of all *PTCH1* exons amplified from peripheral blood DNA failed to identify a pathogenic germline mutation. However, MLPA analysis showed an increase in the copy number of exons 11–17, suggestive of a duplication event involving one copy of the *PTCH1* gene (Fig. 1A). This observation warranted further investigation to establish the effect of exon duplication on gene expression and the phenotype of this patient.

MLPA alone cannot provide an insight as to the precise location and potential functional outcomes of the duplication. Therefore, we next determined the breakpoint of the duplication. An aberrant PCR product was obtained from the genomic DNA of this patient with the P1 and P2 primers (Fig. 1B, lane 3), and sequencing of the PCR product suggested a tandem duplication involving 8 of the 23 coding exons of *PTCH1* (g.39362_58175dup18814 based on NG_007664.1 sequence) (Fig. 1C). The duplicated region was predicted to be 18,814-bp long and the fusion occurred between non-repetitive elements in exon 10 and intron 17 with an overlap of three nucleotides, TGC (Fig. 1D). No microhomology was observed around the duplication junction except for the 3-bp overlap. According to Repeatmasker (http://www.repeatmasker.org), the proximal breakpoint was located 314 bp upstream of an MER5A element and 2,128 bp upstream of an LTR element, LTR85b. The distal breakpoint was 2,773 bp downstream of an MIR3 element. Her parents did not carry the breakpoint sequence, thus this duplication was a de novo event (Fig. 1B, lanes 4 and 5).

To confirm the tandem duplication, we performed Southern blotting using genomic DNA digested with each of the three restriction enzymes and a probe hybridizing to intron 16 (Fig. 2A). As shown in Figure 2B, rearranged bands of expected sizes were detected in the patient but not in a healthy control, verifying the predicted gene structure of the mutant allele.

To investigate the effect of the duplication on the transcription and translation, we next performed an RT-PCR analysis using RNA extracted from lymphoblastoid cell lines derived from the patient and a healthy control. mRNA species harboring a premature termination codon (PTC) usually undergo nonsense-mediated mRNA decay (NMD) [Holbrook et al., 2004]. NMD is a highly conserved surveillance process leading to the detection and selective reduction of PTC-harboring mRNAs to prevent the synthesis of abnormal proteins. Since NMD is a translation-dependent process, the degradation is suppressed by translation inhibitors such as puromycin [Carter et al., 1995]. An aberrant

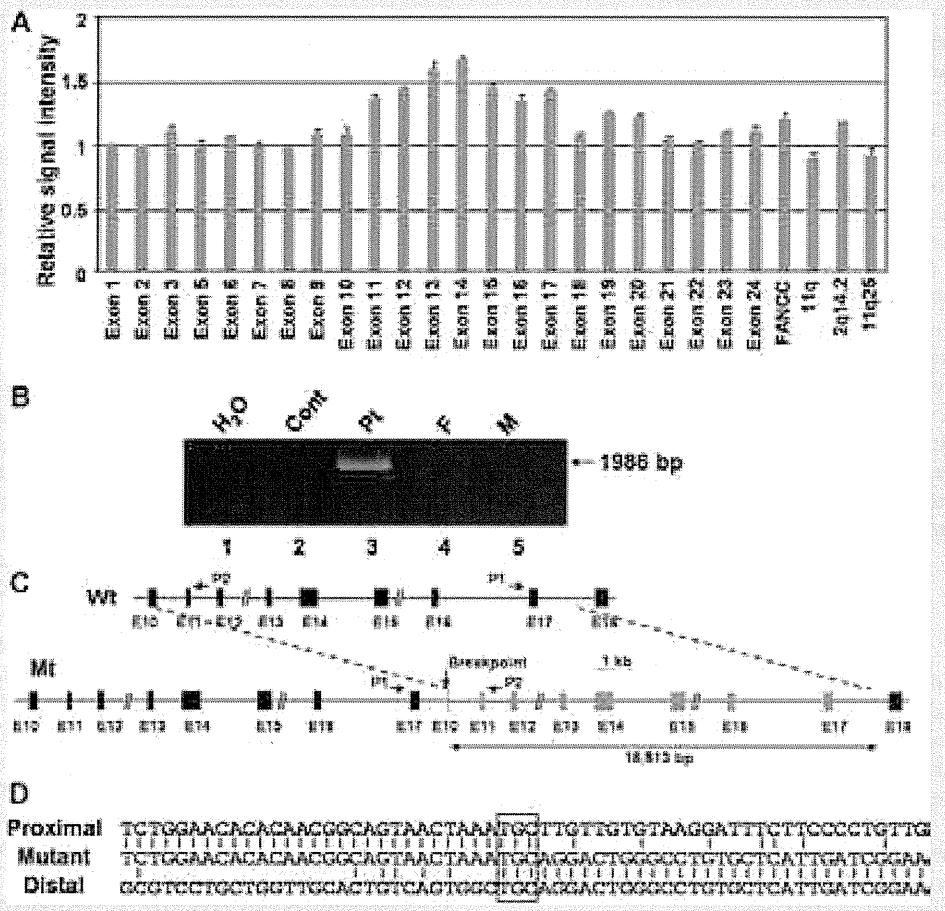

FIG. 1. Assessment of copy number changes. A: MLPA profile. The value of the control average was set to one for all exons. FANCC is an intrachromosomal control while 11q, 2q14.2 and 11q25 are interchromosomal controls. B: Amplified genomic DNA fragment containing a breakpoint. Genomic PCR was performed using the P1 and P2 primers (see panel C) and genomic DNA obtained from the patient (Pt), her father and mother (F and M), and a healthy control (Cont). No template control (H_2O) was also included in the analysis. C: Predicted gene structure. The gene structure of the mutated allele (Mt) was predicted from the PCR result. Exons are depicted as boxes and introns are lines. Duplicated exons are depicted as gray boxes. D: Breakpoint sequence of the junction fragment. The DNA sequence for the duplication-specific junction fragment determined from the PCR product was aligned to the wild-type flanking genome sequence for both proximal and distal breakpoints. The three-nucleotide overlap is depicted as a box.

product was amplified with the P3 and P4 primers specifically from the patient's RNA in the presence of, but not in the absence of puromycin, suggesting the presence of a PTC in the mutant sequence (Fig. 3A). Sequencing of the aberrant product identified a junction between exon 17 and exon 11, generating the duplicated segment composed of exons 11–17 (Fig. 3A,B). According to the junctional sequence, the duplication event was predicted to introduce 12 novel amino acids and then a PTC (Fig. 3C). This provided an explanation for the pathogenesis in this individual.

DISCUSSION

Using MLPA analysis, we identified an approximate 19-kb duplication of the *PTCH1* gene in an individual with NBCCS. The duplicated segment harbored a part of exon 10 and exons 11–17. To date, more than 10 NBCCS patients with a constitutional interstitial deletion involving *PTCH1* have been reported [Shimkets et al., 1996; Olivieri et al., 2003; Haniffa et al., 2004; Midro et al., 2004; Boonen et al., 2005; Fujii et al., 2007; Takahashi et al., 2009; Nagao et al., 2011]. However, this is the first report of a multiexon

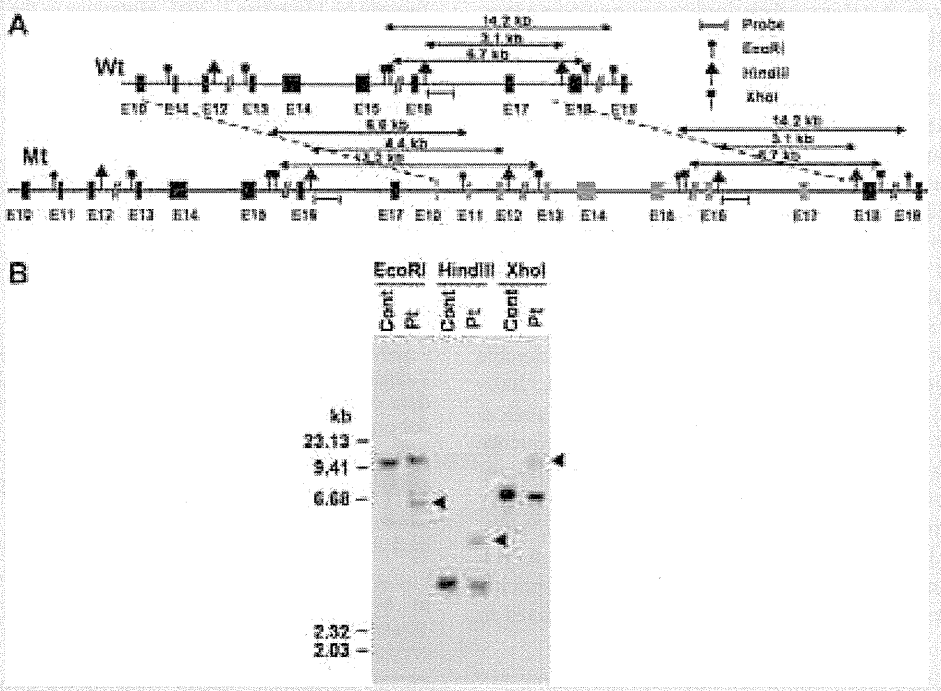

FIG. 2. Southern blot analysis of the patient's genomic DNA. A: Gene structures of both wild-type and mutant (Wt and Mt) alleles are depicted with restriction enzyme sites. The location of the probe and size of the DNA fragment predicted to be detected by Southern blotting are also indicated. B: Autoradiogram of Southern blotting. Genomic DNA of the patient as well as a healthy control was digested with the restriction enzymes indicated at the top and subjected to Southern blotting. Patient-specific rearranged bands are indicated by arrowheads.

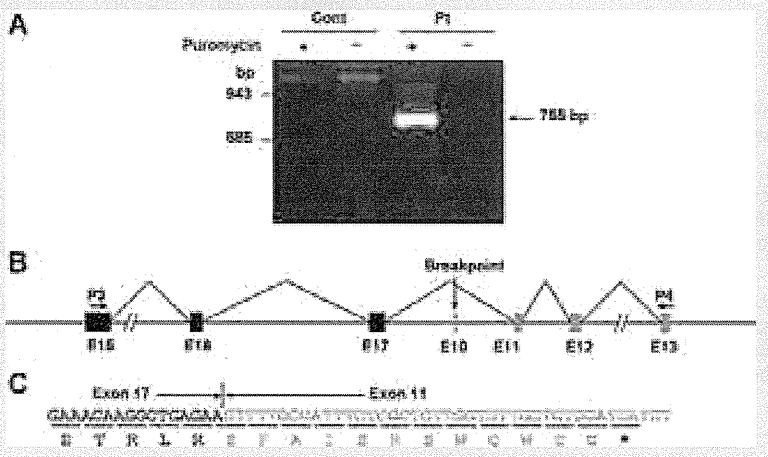

FIG. 3. Analysis of the mutant RNA transcribed from the mutant allele. A: Duplication-specific RT-PCR product. cDNA synthesized from lymphoblastoid cell lines established from the patient and a healthy control cultured in the presence or absence of an NMD inhibitor, puromycin (100 μg/ml), was subjected to RT-PCR using the P3 and P4 primers. B: Genomic structure surrounding the breakpoint. Duplicated exons are depicted by gray boxes. The location of the P3 and P4 primers used for RT-PCR is indicated. The splicing pattern deduced by sequencing the RT-PCR product is also depicted. C: Sequence of the mutant cDNA carrying the breakpoint. Direct sequencing of the duplication-specific RT-PCR product showed that the splicing took place between exon 17 and exon 11, skipping the partial sequence of exon 10 as well as intron 10. Consequently, a frameshift is generated leading to a PTC (*). The duplicated sequence is presented in gray letters.

duplication event that occurred in one of the *PTCH1* alleles. Our findings demonstrate that this tandem duplication results in a loss-of-function mutation and caused NBCCS due to haploinsufficiency of *PTCH1*. Accordingly, this patient did not exhibit manifestations inconsistent with the NBCCS phenotype.

As to the mechanism of the duplication, Alu-Alu-mediated homologous recombination is reported to be responsible for 27% of all segmental duplications in humans [Bailey et al., 2003]. In our study, the comparison of the proximal and distal normal sequences that span the duplication junctions did not identify apparent sequence motifs common to both parental strands at or near the junctions, suggesting that a non-homologous recombination is responsible.

Since large deletions or duplications are found in a considerable fraction of mutation-negative NBCCS patients [Fujii et al., 2007; Nagao et al., 2011], copy number analysis using techniques such as MLPA is strongly recommended to complement DNA sequence analysis. Although cost- and labor-intensive, copy number microarray is another powerful method to detect copy number alterations as reported previously in NBCCS patients [Fujii et al., 2007; Nagao et al., 2011]. When a duplication is detected, RNA analysis is necessary to elucidate the effect on coding since the splicing event taking place in the affected allele is not always predicted in silico.

ACKNOWLEDGMENTS

We greatly appreciate Hiromi Hatsuse for her technical assistance. This research was supported by Science Research Grants for intractable diseases in Japan (H22-intractable diseases-120) from the Ministry of Health, Labour and Welfare, and by a Grant-in-Aid for Scientific Research (20591261) from the Ministry of Education, Culture, Sports, Science and Technology.

REFERENCES

Bailey JA, Liu G, Eichler EE. 2003. An *Alu* transposition model for the origin and expansion of human segmental duplications. Am J Hum Genet 73:823–834.

Boonen SE, Stahl D, Kreiborg S, Rosenberg T, Kalscheuer V, Larsen LA, Tommerup N, Brondum-Nielsen K, Tumer Z. 2005. Delineation of an interstitial 9q22 deletion in basal cell nevus syndrome. Am J Med Genet Part A 132A:324–328.

Carter MS, Doskow J, Morris P, Li S, Nhim RP, Sandstedt S, Wilkinson MF. 1995. A regulatory mechanism that detects premature nonsense codons in T-cell receptor transcripts in vivo is reversed by protein synthesis inhibitors in vitro. J Biol Chem 270:28995–29003.

Fujii K, Kohno Y, Sugita K, Nakamura M, Moroi Y, Urabe K, Furue M, Yamada M, Miyashita T. 2003. Mutations in the human homologue of *Drosophila patched* in Japanese nevoid basal cell carcinoma syndrome patients. Hum Mutat 21:451–452.

Fujii K, Ishikawa S, Uchikawa H, Komura D, Shapero MH, Shen F, Hung J, Arai H, Tanaka Y, Sasaki K, Kohno Y, Yamada M, Jones KW, Aburatani H, Miyashita T. 2007. High-density oligonucleotide array with sub-kilobase resolution reveals breakpoint information of submicroscopic deletions in nevoid basal cell carcinoma syndrome. Hum Genet 122: 459–466.

Gorlin RJ. 1987. Nevoid basal-cell carcinoma syndrome. Medicine (Baltimore) 66:98–113.

Hahn H, Wicking C, Zaphiropoulous PG, Gailani MR, Shanley S, Chidambaram A, Vorechovsky I, Holmberg E, Unden AB, Gillies S, Negus K, Smyth I, Pressman C, Leffell DJ, Gerrard B, Goldstein AM, Dean M, Toftgard R, Chenevix-Trench G, Wainwright B, Bale AE. 1996. Mutations of the human homolog of Drosophila *patched* in the nevoid basal cell carcinoma syndrome. Cell 85:841–851.

Haniffa MA, Leech SN, Lynch SA, Simpson NB. 2004. NBCCS secondary to an interstitial chromosome 9q deletion. Clin Exp Dermatol 29:542–544.

Holbrook JA, Neu-Yilik G, Hentze MW, Kulozik AE. 2004. Nonsense-mediated decay approaches the clinic. Nat Genet 36:801–808.

Johnson RL, Rothman AL, Xie J, Goodrich LV, Bare JW, Bonifas JM, Quinn AG, Myers RM, Cox DR, Epstein EH Jr, Scott MP. 1996. Human homolog of *patched*, a candidate gene for the basal cell nevus syndrome. Science 272:1668–1671.

Midro AT, Panasiuk B, Tumer Z, Stankiewicz P, Silahtaroglu A, Lupski JR, Zemanova Z, Stasiewicz-Jarocka B, Hubert E, Tarasow E, Famulski W, Zadrozna-Tolwinska B, Wasilewska E, Kirchhoff M, Kalscheuer V, Michalova K, Tommerup N. 2004. Interstitial deletion 9q22.32-q33.2 associated with additional familial translocation t(9;17)(q34.11;p11.2) in a patient with Gorlin-Goltz syndrome and features of Nail-Patella syndrome. Am J Med Genet Part A 124A:179–191.

Nagao K, Fujii K, Saito K, Sugita K, Endo M, Motojima T, Hatsuse H, Miyashita T. 2011. Entire *PTCH1* deletion is a common event in point mutation-negative cases with nevoid basal cell carcinoma syndrome in Japan. Clin Genet 79:196–198.

Olivieri C, Maraschio P, Caselli D, Martini C, Beluffi G, Maserati E, Danesino C. 2003. Interstitial deletion of chromosome 9, int del(9)(9q22.31-q31.2), including the genes causing multiple basal cell nevus syndrome and Robinow/brachydactyly 1 syndrome. Eur J Pediatr 162:100–103.

Shimkets R, Gailani MR, Siu VM, Yang-Feng T, Pressman CL, Levanat S, Goldstein A, Dean M, Bale AE. 1996. Molecular analysis of chromosome 9q deletions in two Gorlin syndrome patients. Am J Hum Genet 59: 417–422.

Takahashi C, Kanazawa N, Yoshikawa Y, Yoshikawa R, Saitoh Y, Chiyo H, Tanizawa T, Hashimoto-Tamaoki T, Nakano Y. 2009. Germline *PTCH1* mutations in Japanese basal cell nevus syndrome patients. J Hum Genet 54:403–408.